J Mater Sci (2010) 45:6574–6585
DOI 10.1007/s10853-010-4746-3

Size-controllable synthesis of chromium oxyhydroxide nanomaterials using a soft chemical hydrothermal route

Jing Yang · Adrian G. Baker · Hongwei Liu · Wayde N. Martens · Ray L. Frost

Received: 14 March 2010 / Accepted: 28 June 2010 / Published online: 15 July 2010

Abstract Chromium oxyhydroxide nanomaterials were synthesised through a simple soft chemical hydrothermal method. The chromium oxyhydroxide materials display platelet morphology with clear edges, ~11 nm in diameter. CrO(OH) nanomaterials synthesised under different conditions were fully characterised by X-ray diffraction (XRD), transmission electron microscopy (TEM) combined with selected area electron diffraction (SAED), scanning electron microscopy (SEM), BET specific surface area analysis, X-ray photoelectron spectroscopy (XPS) and thermal gravimetric analysis (TGA). Bonding of the trivalent chromium from the oxyhydroxide nanomaterials was defined through the analysis of their high resolution XPS spectra for Cr $2p_{3/2}$ and O 1s. The thermal stability of the nanomaterials CrO(OH) was established. This research has developed methodology for the synthesis of chromium oxyhydroxide nanoplates.

Introduction

Transition metal oxides are important materials in industry, as well as their use as heterogenous catalysts, both as support materials as well as active components. Special attention has been focused on the formation and properties of chromia (Cr_2O_3), which is important in specific applied applications such as in high-temperature resistant materials [1–3], solar energy collectors [4–6], liquid crystal displays [7, 8] and catalysts [9–12]. Cr_2O_3 and CrO(OH) were also detected in rust formed by corrosion of Cr-containing steels, and extensively studied [13–16]. Cr_2O_3 and CrO(OH) are observed to be in a similar relationship to cobalt oxyhydroxide to oxides [17]. Chromium oxyhydroxide is a principal precursor for synthesis of chromium oxides. The morphology and nanosize of the oxyhydroxide can be retained to the oxides through a topotactical relationship [17–20]. Therefore, studies on controllable synthesis and characterisation for CrO(OH) nanomaterials are important for the synthesis and application of Cr_2O_3 nanomaterials in industry.

It is reported that there are three currently known synthetic polymorphs of CrO(OH): trigonal α-CrO(OH) with a space group of *R*3*m*, orthorhombic *β*-CrO(OH) with a space group of *Pnnm* and *γ*-CrO(OH) with a space group of *Cmcm* [21]. Approved in 1977 by the Commission on New Minerals and Mineral Names of the International Mineralogical Association (IMA-CNMMN), the naturally occurring chromium oxyhydrates include three species: bracewellite (orthorhombic CrO(OH)), guyanite (orthorhombic *β*-CrO(OH)) and grimaldiite (trigonal CrO(OH)) [21]. So far, limited research has been undertaken on the synthesis and industrial application of CrO(OH) and Cr_2O_3 nanomaterials.

By reducing potassium chromate with hydrogen and then calcining the resultant intermediate, which consists of $Cr(OH)_3{\cdot}nH_2O$ and CrO(OH), the ultra-fine chromia (Cr_2O_3) powder with a mean diameter of 0.3 μm has been prepared [22]. The preparation of chromium oxide is of considerable interest since this compound is a component of many oxide-type catalysts. Cr(III)–Fe(III)-(oxy)

Electronic supplementary material The online version of this article (doi:10.1007/s10853-010-4746-3) contains supplementary material, which is available to authorized users.

J. Yang · A. G. Baker · H. Liu · W. N. Martens · R. L. Frost (✉)
Chemistry Discipline, Faculty of Science and Technology, Queensland University of Technology, GPO Box 2434, Brisbane, QLD 4001, Australia
e-mail: r.frost@qut.edu.au

hydroxides have been reported by Tang et al. [23]. It is found that the Cr end member sizing around 1 nm is likely to be amorphous with aspects of local structure similar to γ-CrO(OH). Landau et al. [24] and Rotter et al. [9] reported catalytic materials based on chromia aerogel, which consists of 1–2 nm CrO(OH) nanocrystals with very high surface area. $CrO(OH)\cdot 2H_2O$ nanocrystals of 3–5 nm in diameter were prepared by critical CO_2 extraction of the urea-assisted wet chromia gel mixture at 373 K in vacuum [25, 26]. As reported, metal oxides can be formed through the thermal dehydration of their corresponding oxyhydroxides, which can preserve the texture of their precursors [20, 27–29]. It is reported that hydrated chromium oxides are mostly used as initial compounds for the synthesis of chromium oxides [30]. As the important precursor for chromium oxides through thermal treating, the thermal stability and decomposition process of chromium hydroxide or chromium oxide hydroxide has been investigated [30–35]. However, not much work has been undertaken on the thermal stability of nanoscaled CrO(OH) materials.

Possible industrial applications of CrO(OH) and Cr_2O_3 materials depend on their chemical, physical and micro-/nano-structure properties. Generally the properties of materials can be modified by their synthesis conditions. Therefore, researchers have tried to establish the relation between the properties of chromium oxide materials and synthesis conditions. In this study, a simple soft chemical method is used and well-crystalline chromium oxide hydroxide nanoplates with an average size of 11 nm were successfully synthesised. The synthetic CrO(OH) nanoparticles are very uniform in morphology and size. Detailed discussion is presented in the text, particularly on the controllable synthesis, as well as material structure, surface properties and their thermal stabilities of the synthetic CrO(OH) nanomaterials. The aim of this research is to investigate the influence of experimental procedures on the synthesis and properties of chromium oxyhydroxide nanomaterials.

Experimental

Material synthesis

Typically, 15 g of $Cr(NO_3)_3\cdot 9H_2O$ was dissolved in 75 mL ultra pure water, and 28% ammonia was diluted to 10% solution. At room temperature 10% ammonia solution was added at a rate of 1 mL min^{-1} into $Cr(NO_3)_3$ solution with vigorous stirring. Ammonia solution addition ceased when the pH of the reaction mixture reached the desired values (5.0, 7.5 or 10.0). The reaction mixture was then kept stirring constantly in air at room temperature for 0.5 h. The obtained gel was centrifuged and washed at 13000 rpm for 10 min, for three times. The washed wet gel was transferred into a glass beaker (25 mL). The beaker was placed into a Teflon vessel, 2 mL ultra pure water was poured into the bottom of the Teflon vessel. The Teflon vessel was then sealed and hydrothermally treated at 170 °C for 12 h $\sim$4 days. The resultant products were washed with ultrapure water and collected by centrifugation (at 13000 rpm for 10 min, repeated 3 times). Samples were dried at 65 °C overnight. Samples ID used in this paper and their preparation conditions are shown in Table 1.

X-ray diffraction

X-ray diffraction (XRD) patterns were collected using a PANalytical X'Pert PRO X-ray diffractometer (radius: 240.0 mm). Incident X-ray radiation was produced from a line focused PW3373/10 Cu X-ray tube, operating at 40 kV and 40 mA, with Cu Kα radiation of 1.540596 Å. The

Table 1 Samples ID used in this paper and their preparation conditions

Sample ID	pH for wet gel precipitate	HT temp. (°C)	HT duration	TGA products
ppt-5.0	5.0	–	–	–
ppt-7.5	7.5	–	–	–
ppt-10.0	10.0	–	–	–
CrO(OH)-5.0	5.0	170	12 h	–
gel-7.5-a	7.5	170	12 h	–
gel-10.0-a	10.0	170	12 h	–
CrO(OH)-7.5	7.5	170	4 days	–
CrO(OH)-10.0	10.0	170	4 days	–
ppt-5.0-TGA	5.0	–	–	Yes
CrO(OH)-5.0-TGA	5.0	170	12 h	Yes
CrO(OH)-7.5-TGA	7.5	170	4 days	Yes
CrO(OH)-10.0-TGA	10.0	170	4 days	Yes

HT hydrothermal treatment

incident beam passed through a 0.04 rad soller slit, a 1/2° divergence slit, a 15 mm fixed mask and a 1° fixed anti-scatter slit.

Scanning electron microscopy

The specimens were mounted on scanning electron microscopy (SEM) mounts with carbon tape and coated with a thin layer of evaporated gold. The secondary electron images were obtained using a scanning electron microscope (FEI Quanta 200 SEM, FEI Company, Hillsboro, Oregon, USA), operating at 30 kV.

Transmission electron microscopy

A Philips CM20 transmission electron microscope (TEM) at 160 kV was used to investigate the morphology of the as-prepared samples. All samples were ultrasonically dispersed in absolute ethanol solution, and then dropped on copper grids. Selected area electron diffraction (SAED) was performed via the same TEM.

Specific surface area analysis

Surface area analyses based upon N_2 adsorption/desorption techniques were analysed on a Micrometrics Tristar 3000 automated gas adsorption analyser. Before the analysis, samples were pre-treated at 110 °C under the flow of N_2 on a Micrometrics Flowprep 060 degasser.

X-ray photoelectron spectroscopy (XPS)

Data was acquired using a Kratos Axis ULTRA X-ray photoelectron spectrometer incorporating a 165 mm hemispherical electron energy analyser. The incident radiation was Monochromatic Al Kα X-rays (1486.6 eV) at 150 W (15 kV, 10 mA) and at 45° to the sample surface. Photoelectron data was collected at take off angle of $\theta = 90°$. Narrow high resolution scans were run with 0.05 eV steps and 250 ms dwell time. Base pressure in the analysis chamber was 1.0×10^{-9} Torr and during sample analysis 1.0×10^{-8} Torr.

A small amount of each finely powdered sample was carefully applied to double sided adhesive tape on a standard Kratos Axis Ultra sample bar. This was attached to the sample rod of the Load Lock system for initial evacuation to $\sim 1 \times 10^{-6}$ Torr. The sample bar was then transferred to the UHV sample analysis chamber (SAC) for collection of X-ray photoemission spectra. Spectra were subjected to a Shirley baseline. Various data handling procedures were carried out using the CasaXPS version 2.3.14 software.

Thermal gravimetric analysis

Thermal decomposition of the samples was carried out in a TA® Instruments incorporated high resolution thermo gravimetric analyser (series Q500) in a flowing nitrogen atmosphere (60 cm^3 min^{-1}). Approximately 50 mg of each sample underwent thermal analysis, with a heating rate of 5 °C min^{-1}, with resolution of 6 from 25 to 1000 °C. With the isothermal, isobaric heating program of the instrument the furnace temperature was regulated precisely to provide a uniform rate of decomposition in the main decomposition stage. The TGA instrument was coupled to a Balzers (Pfeiffer) mass spectrometer for gas analysis. Only water vapour, nitric oxide, carbon dioxide and oxygen were analysed. In the MS figures, e.g. Fig. 9, a background of broad peaks may be observed. This background occurs for all the ion current curves. The background becomes more prominent as the scale expansion is increased. It is considered that this background may be due to the loss of chemicals which have deposited in the capillary which connects the TA instrument to the MS.

Results and discussion

Structure and morphology

The XRD patterns of the colloidal precipitation obtained under different pH values and of the samples after being hydrothermally treated at 170 °C for 12 h are shown in Fig. 1. Prior to the hydrothermal treatment (HT), the colloidal chromium hydroxide materials resulting from reaction of $Cr(NO_3)_3$ and NH_4OH solutions, noted as ppt-5.0, ppt-7.5 and ppt-10.0 separately, were amorphous. No XRD peaks were observed for these precipitated samples. This agrees with literature, which reported that the hydrogel

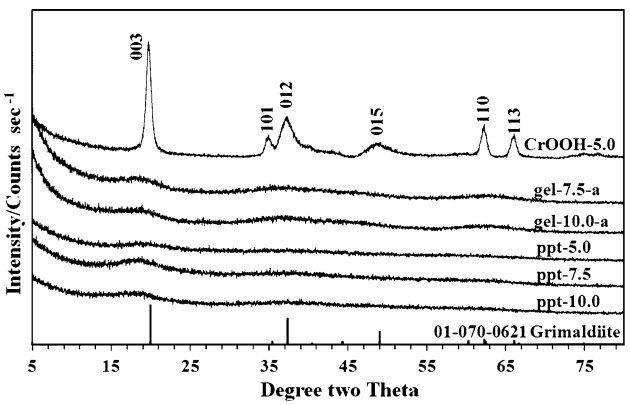

Fig. 1 XRD patterns of ppt-5.0, ppt-7.5, ppt-10.0, CrO(OH)-5.0, gel-7.5-a and gel-10.0-a. XRD pattern from literature: JCPDS card No. 01-070-0621 Grimaldiite

obtained from the neutralisation of Cr^{3+} ions is usually amorphous or poorly crystalline [36, 37]. The conversion process from colloidal chromium precipitate to crystalline CrO(OH) was found to be significantly affected by the precipitation conditions. After a HT at 170 °C for 12 h, only the sample precipitated at pH = 5.0 was transformed to well-crystalline phase, noted as CrO(OH)-5.0; while the other two samples, which precipitated at pH 7.5 and 10.0, remain amorphous, as shown in Fig. 1. A well defined XRD pattern for CrO(OH)-5.0 was observed and all diffraction peaks were perfectly indexed to rhombohedral CrO(OH), which has the mineral name Grimaldiite, with a space group of *R*3*m* (JCPDS card No. 01-070-0621). The parameters of the rhombohedral unit cell of Grimaldiite are: $a = 2.979$ Å, $c = 13.370$ Å [38]. No XRD peaks representing other crystalline phases were detected, indicating a high purity of the resultant crystalline solid by a hydrothermal conversion process. Based on XRD results, the average crystallite size of sample CrO(OH)-5.0 was 11 nm by application of the Scherrer equation. The Scherrer equation is $D = K\lambda/\beta\cos\theta$, where D is the crystalline size (nm), K is the Scherrer constant, which has a value of 0.89, λ is the X-ray wavelength (nm), β is the observed peak width and θ is the diffraction angle.

Figure 2 compares the SEM images of materials synthesised at pH = 5.0 before and after the HT at 170 °C. As shown in Fig. 2a, the colloidal precipitate appears to be non-crystallized lumpy aggregates. A similar SEM morphology of natural amorphous γ-CrO(OH) was reported by Shpachenko et al. when they studied the genesis and compositional characteristics of natural γ-CrO(OH) [21]. After 12-h HT, the morphology of the crystallized nanostructures of CrO(OH) was observed to be nano-particles (Fig. 2b). The average diameter of these spherical nanoparticles was 50 nm.

As discussed above, after a HT for 12 h, only the precipitate obtained at acidic conditions (pH = 5.0) transformed into crystalline CrO(OH) material. In comparison, the precipitates obtained at pH = 7.5 and 10.0 were hydrothermally treated for a longer period of time. The products after 4-day treatment were characterised and shown to be CrO(OH) by XRD, Fig. 3. Peaks of both XRD patterns can be well indexed and matched with the peaks of the grimaldiite standard pattern (JCPDS card No. 01-070-0621). This indicates that a much longer hydrothermal duration time is required to promote the conversion to crystalline CrO(OH) from the precipitates obtained in neutral (pH = 7.5) and alkaline (pH = 10) conditions. However, the CrO(OH) product from alkaline precipitation condition shows a much better crystallinity. On the basis of the broadening of diffraction lines, it was estimated that the mean crystallite size of sample CrO(OH)-10.0 was 12 nm. In the XRD pattern of CrO(OH)-7.5, low intensity of XRD reflections were found at positions exactly corresponding to grimaldiite structure. In the XRD pattern of CrO(OH)-7.5, low intensity of XRD reflections were found at positions exactly corresponding to grimaldiite structure. These lower XRD intensity and large broadening of corresponding

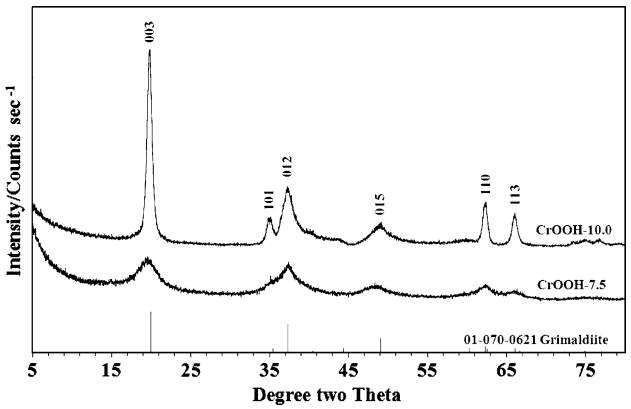

Fig. 3 XRD patterns of CrO(OH)-10.0 and CrO(OH)-7.5. XRD pattern from literature: JCPDS card No. 01-070-0621 Grimaldiite

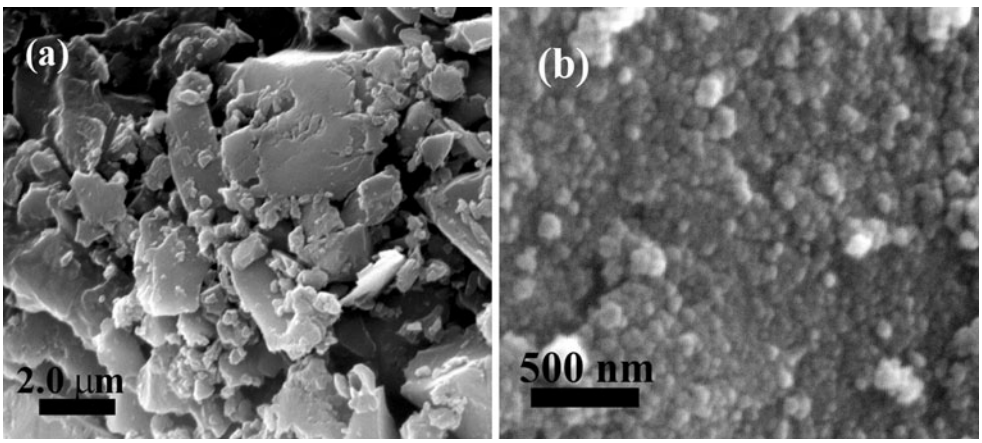

Fig. 2 SEM images of (**a**) ppt-5.0 and (**b**) CrO(OH)-5.0

peaks indicate that crystals of CrO(OH)-7.5 are of significantly lower crystal, even after a longer (4 days) HT.

It is noted that particle size differs from crystallite size by definition; however, in the case of very small particles their size is often comparable with the crystallite size, as estimated by the Scherrer formula. Typical TEM images of the three crystalline CrO(OH) materials synthesised under different conditions are shown in Fig. 4. The resulting samples from acidic and alkaline conditions appear as nanoplates. The average size in diameter for sample CrO(OH)-5.0 is measured to be 10 nm, while for CrO(OH)-10.0 the average measured size is 12 nm. This slight increase in size is considered to be due to longer hydrothermal crystal growth duration. It is noted that size of the crystals observed under transmission electron microscope is in excellent agreement with the results calculated by Scherrer equation determined by XRD data.

In order to increase our understanding of the morphology of these CrO(OH) nanocrystals, high resolution TEM (HRTEM) with a double tilt holder was utilised. Detailed high resolution imaging micrographs were included in the supporting information. Figure 4c presents one HRTEM image for CrO(OH)-7.5 and the SAED of the corresponding area has been inserted. It is revealed that no extra dimensionality of the nano-platelets can be observed, which means that the nanoparticles were in a plate shape, instead of being bulk crystals. The particles size of CrO(OH)-7.5 material as determined from this HRTEM image was measured to be 4 nm. This is in excellent agreement with the results based on the Scherrer equation. An area in the HRTEM image was found showing no interference patterns under the HRTEM detection, thus indicating there was an amorphous fraction in the sample.

For CrO(OH)-5.0 the SAED pattern of the corresponding area in Fig. 4a appears in rings, which indicates that the hydrothermal synthesis yielded polycrystalline nanomaterials of CrO(OH). The nanoplates of synthesised CrO(OH) exhibited excellent crystallinity, which is confirmed by the results of the XRD investigation. The SAED pattern (Fig. 4b) matched well with that in the XRD study, and the

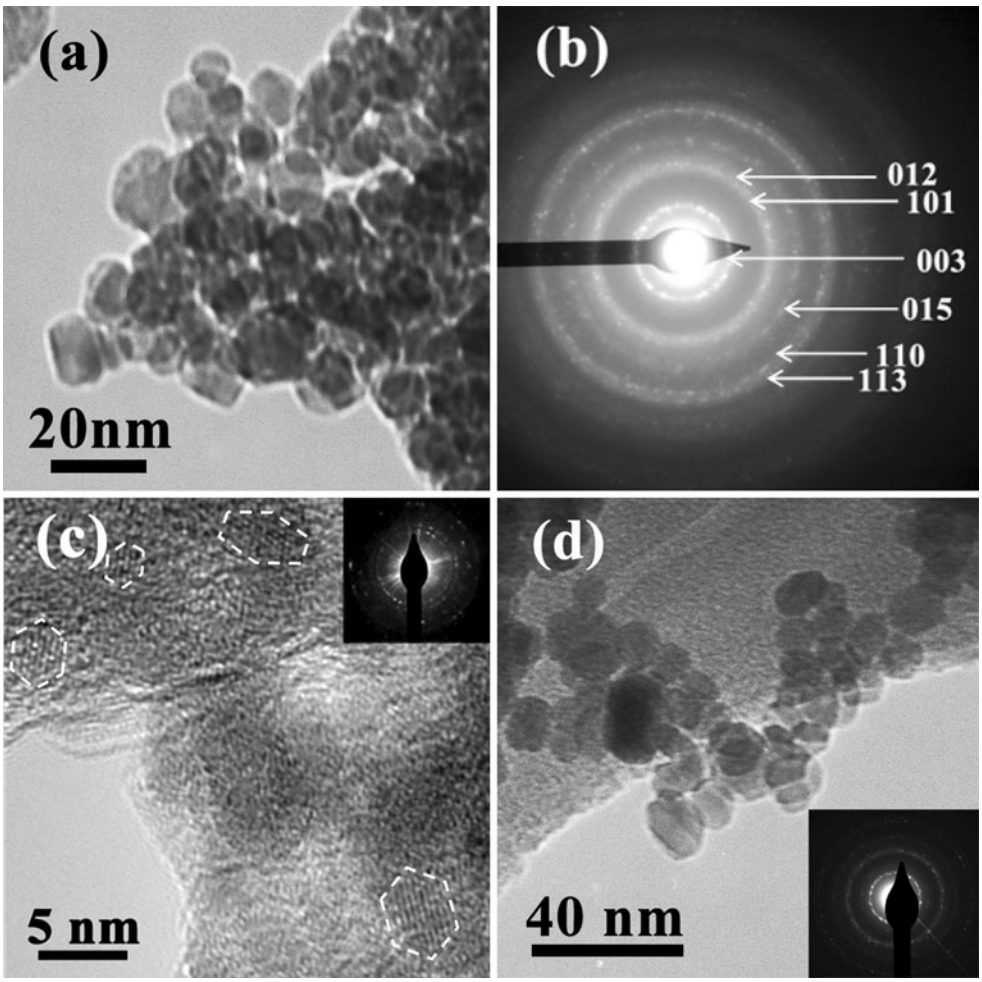

Fig. 4 (**a**) TEM image of CrO(OH)-5.0; (**b**) SAED result of the corresponding area in **a**; (**c**) TEM images of CrO(OH)-7.5 and its SAED result (*inset*); (**d**) CrO(OH)-10.0 and its SAED result (*inset*)

indexing of the ring pattern indicated that the nanoplates possessed a crystal structure consistent with the rhombohedral form of CrO(OH). It is observed that there are individual bright spots in the rings, which indicate large and well formed crystals in the sample. This observation is in harmony with the corresponding TEM image.

Surface analysis

N_2 adsorption studies

The N_2 adsorption–desorption measurement at a liquid N_2 temperature of 77 K was applied to study the porosity and textural properties of the CrO(OH) nanomaterials precipitated under different pH conditions. Figure 5 depicts the N_2 adsorption–desorption isotherms of all the samples, all of which exhibit a type IV sorption behaviour, indicating the presence of mesoporous structural characteristic according to the classification of IUPAC [39]. Type IV isotherm possesses a hysteresis loop, the lower branch of which represents measurements obtained by progressive addition of vapour to the system and the upper branch by progressive withdrawal [40]. The apparent step in the adsorption branch combined with the sharp decline in the desorption branch is an obvious verification in the presence of mesoporosity. As shown in Fig. 5, the adsorption of N_2 of CrO(OH)-7.5 is much higher than that of the other two samples, which indicates that CrO(OH)-7.5 possesses a higher specific surface area. It is known that the specific

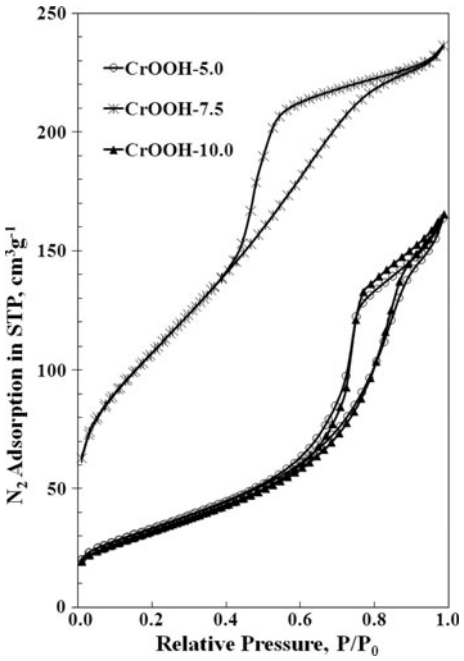

Fig. 5 N_2 adsorption/desorption isotherms for CrO(OH)-5.0, CrO(OH)-7.5 and CrO(OH)-10.0

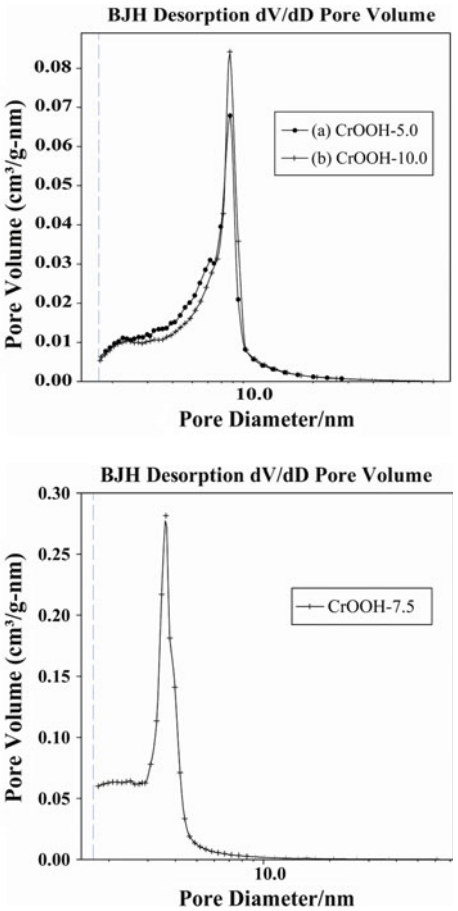

Fig. 6 Pore size distribution study for CrO(OH)-5.0, CrO(OH)-7.5 and CrO(OH)-10.0

surface area, pore volume and pore size distribution can be calculated and compared from the N_2 adsorption isotherms of materials [40]. A pore size distribution is presented in Fig. 6, which shows that the distribution of pore size is mostly in the mesopore region (pore size between 2 and 50 nm) due to the single hysteresis loop. The textural properties of CrO(OH)-7.5 synthesised under a neutral condition are given in Table 2 as follows: a BET specific surface area of 384 $m^2\ g^{-1}$ with a BJH mean pore diameter of 3.5 nm (within mesopore region) and desorption cumulative pore volume of 0.33 $cm^3\ g^{-1}$. CrO(OH)-5.0 and CrO(OH)-10.0, precipitated, respectively, under the acidic and alkaline conditions, present similar patterns of N_2 adsorption isotherm and pore size distribution to those of sample CrO(OH)-7.5. However, their textural properties show the following changes: CrO(OH)-5.0 has a BET specific surface area of 119 $m^2\ g^{-1}$ with a BJH mean pore diameter of 6.7 nm (within mesopore region) and desorption cumulative pore volume of 0.25 $cm^3\ g^{-1}$, while CrO(OH)-10.0 has a BET specific surface are of 115 $m^2\ g^{-1}$ with a BJH mean pore diameter of 6.9 nm (within mesopore region) and desorption cumulative pore

Table 2 BET specific surface area (S_{BET}), pore volume (V_p) and pore diameter for synthesised CrO(OH) nanomaterials

Sample ID	S_{BET} (m^2 g^{-1})	V_p^a (cm^3 g^{-1})	Mean D (nm)	
			BET[b]	BJH[c]
CrO(OH)-5.0	119.09	0.25	8.5	6.7
CrO(OH)-10.0	114.63	0.26	8.9	6.9
CrO(OH)-7.5	384.14	0.33	3.8	3.5

[a] BJH desorption cumulative pore volume of pores between 1.7 and 300 nm in diameter

[b] Adsorption average pore diameter (4*V*/*A* by BET)

[c] Barrett–Joyner–Halenda (BJH) desorption average pore diameter (4*V*/*A*)

volume of 0.26 cm^3 g^{-1}. These changes can be attributed to the difference of the crystalline size for the nanomaterials: the increase of the crystals/particle size leads to decrease in the specific surface area and cumulative pore volume, but increase in the mean pore diameter. By comparison, the calculated mean pore size of materials is found to be slightly smaller than the crystalline size observed from XRD and TEM studies; since it is the inter crystalline porosity that is studied by this N_2 adsorption–desorption measurement.

X-ray photoelectron spectroscopy (XPS)

To further determine the surface chemical composition and the chemical states of the prepared nanomaterials, XPS analysis was carried out. XPS has been widely applied for the investigation of the top few layers of material surfaces with partially filled valence band. Spectral results from the interaction with metal valence electrons can provide chemical environment information about the metal ions. For the transition metal element chromium, high resolution Cr 2p spectrum shows spin–orbit splitting into $2p_{1/2}$ and $2p_{3/2}$ components [41, 42], and both components qualitatively contain the same chemical information. Therefore, in this study only the higher intensity Cr $2p_{3/2}$ bands were curve-fitted and discussed. The high resolution XPS spectra of Cr $2p_{3/2}$ and O 1s of the chromium nanomaterials synthesised under various conditions are compared in Fig. 7, and their curve-fitted results are summarised in Table 3. All the spectra were referenced to the adventitious carbon of binding energy (BE) 285.0 eV.

High resolution XPS spectra for Cr 2p are often involved because of the complex multiplet and spin–orbit splitting; however, their decomposition can reveal all the component peaks. XPS spectra may be fitted in different ways and this may affect the interpretation of the XPS data. Studies were performed on simple compounds to obtain reference data for the proper peak assignment [28]. In this study, as shown in Fig. 7, the precipitate sample ppt-5.0 and the three hydrothermally treated samples: CrO(OH)-5.0, CrO(OH)-7.5 and CrO(OH)-10.0 exhibit XPS Cr $2p_{3/2}$ spectra that are very similar in nature to each other with virtually identical peak profiles. Three peaks are required to curve fit the Cr $2p_{3/2}$ XPS spectra of all the four samples,

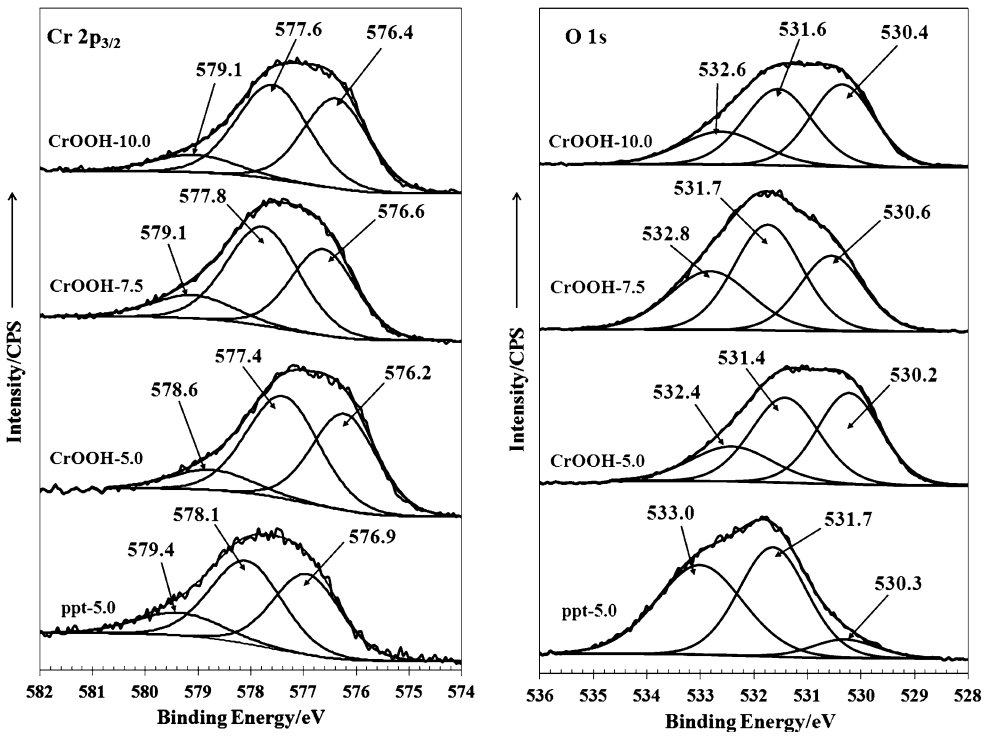

Fig. 7 XPS high resolution spectra of Cr $2p_{3/2}$ and O 1s for ppt-5.0, CrO(OH)-5.0, CrO(OH)-7.5 and CrO(OH)-10.0

Table 3 Results for curve-fitted binding energies and their atomic contents (at.%) of highly resolved Cr $2p_{3/2}$ and O 1s XPS spectra shown in Fig. 7 for sample ppt-5.0, CrO(OH)-5.0, CrO(OH)-7.5 and CrO(OH)-10.0

Samples	Cr $2p_{3/2}$ (eV)			O 1s (eV)		
	Cr1	Cr2	Cr3	O1	O2	O3
ppt-5.0	576.9 (40.8%)	578.1 (44.7%)	579.4 (14.5%)	530.3 (7.0%)	531.7 (45.6%)	533.0 (47.4%)
CrO(OH)-5.0	576.2 (41.0%)	577.4 (48.3%)	578.6 (10.7%)	530.2 (40.4%)	531.4 (40.1%)	532.4 (19.5%)
CrO(OH)-7.5	576.6 (38.5%)	577.8 (48.7%)	579.1 (12.8%)	530.6 (28.7%)	531.7 (42.9%)	532.8 (28.4%)
CrO(OH)-10.0	576.4 (41.7%)	577.6 (48.2%)	579.1 (10.1%)	530.4 (39.7%)	531.6 (39.6%)	532.6 (20.7%)

which indicates that there were three chemical states for chromium. The first component (Cr 1) at around 576.4 eV used for curve fitting is assigned to Cr^{3+} trivalent oxide state, a second one (Cr 2) at around 577.6 eV is associated to the trivalent hydroxide state, which has been well documented [43–45]. The third fitted BE with atomic content of $\sim$10% is found at round 579.0 eV, which is slightly higher than the reported BE for normal Cr(III) from chromium hydroxide, and much lower than that for Cr(VI) [46, 47]. However, it is reported that the BE for chromium could be slightly higher when the element has a more complex load in the compound [48, 49]. Therefore, the third fitted component (Cr 3) observed in this study is considered to be trivalent chromium combined with additional ligands, such as OH^- and H_2O ligands present in the surface of the synthesised materials. The observed slight increase in the Cr $2p_{3/2}$ binding energies for ppt-5.0 can also be explained by the more complex load to chromium in this precipitate sample before HT. The atomic ratios for three kinds of fitting Cr components are very close, where Cr 2 has the biggest portion.

As shown in Fig. 7, the O 1s spectrum for CrO(OH)-5.0 could also be fitted with three peaks: O 1 at 530.2 eV corresponding to O^{2-} in CrO(OH), O 2 at 531.4 eV corresponding to OH^- in oxyhydroxide or hydroxide, and a third peak, O 3 at 532.4 eV corresponding to oxygen in water, which are in excellent agreement with the values reported in literature [47, 50, 51]. The qualitative analysis shows that O 1 and O 2 obtained similar ratios (40.0 and 40.1%) in the sample, which is consistent with their atom ratio of 1:1 in CrO(OH). This illustrates the main composition in CrO(OH)-5.0 is chromium oxyhydroxide, with minimal chromium hydroxide. The O 1s spectrum for CrO(OH)-10.0 shows similar shape and curve-fitted results as CrO(OH)-5.0. The absence of significant BE shifts between these two chromium nanomaterials suggests that the chemical nature of the elements in the top-most surface layers is very similar, and that CrO(OH)-10.0 mainly contains CrO(OH) as well. In the O 1s spectra for ppt-5.0 and CrO(OH)-7.5, three peaks can also be fitted and assigned to O^{2-}, OH^- and H_2O, respectively. Their binding energies are slightly higher than that of CrO(OH)-5.0. However, a decrease of atomic contents for O 1 and an increase of atomic contents for O 2 are observed in CrO(OH)-7.5, which suggests a lower content of CrO(OH) in the sample. One possible interpretation of this CrO(OH) content variation is that the amorphous precipitates obtained at neutral condition (pH = 7.5) require longer HT to form a better CrO(OH) phase. This finding is consistent with the XRD and TEM observations, which reflect the fact that CrO(OH)-7.5 contains non-CrO(OH) amorphous phase which is not very well-crystalline. Moreover, in the O 1s spectrum for ppt-5.0, a low atomic content of O 1 is observed (7%), while the atomic percentage for O 2 is 45.6%. Therefore, without HT, at pH = 5.0, the formula of the amorphous materials is represented by $CrO_{0.13}(OH)_{1.87}$. High atomic contents for O 2 from OH^- and O 3 from H_2O are observed, which confirm that the precipitate contains large amounts of hydroxide and water in the structure.

Thermogravimetric analysis

The thermogravimetric and differential thermogravimetric analysis of the synthesised chromium materials are presented in Fig. 8, which shows the TG and dTG curves for samples obtained in different conditions: (a) pH = 5.0, precipitate without HT, noted as sample A; (b) pH = 5.0, HT for 12 h, noted as sample B; (c) pH = 7.5, HT for 4 days, noted as sample C; (d) pH = 10.0, HT for 4 days, noted as sample D. Thermal decomposition properties of the synthesised materials are discussed in details as follows.

Figure 8a shows the thermal decomposition of amorphous chromium hydroxide gel precipitated under pH = 5.0 at room temperature (A). Two sharp dTG peaks are observed at 149 and 177 °C with mass losses of 6.94 and 21.54%, respectively. These two mass loss steps are attributed to the loss of water in the structure. A second mass loss step is observed at 439 °C with a mass loss of 5.75%, which is attributed to the dehydroxylation of the compound. A minor mass loss observed at 77 °C is attributed to the desorption of water. Ratnasamy and

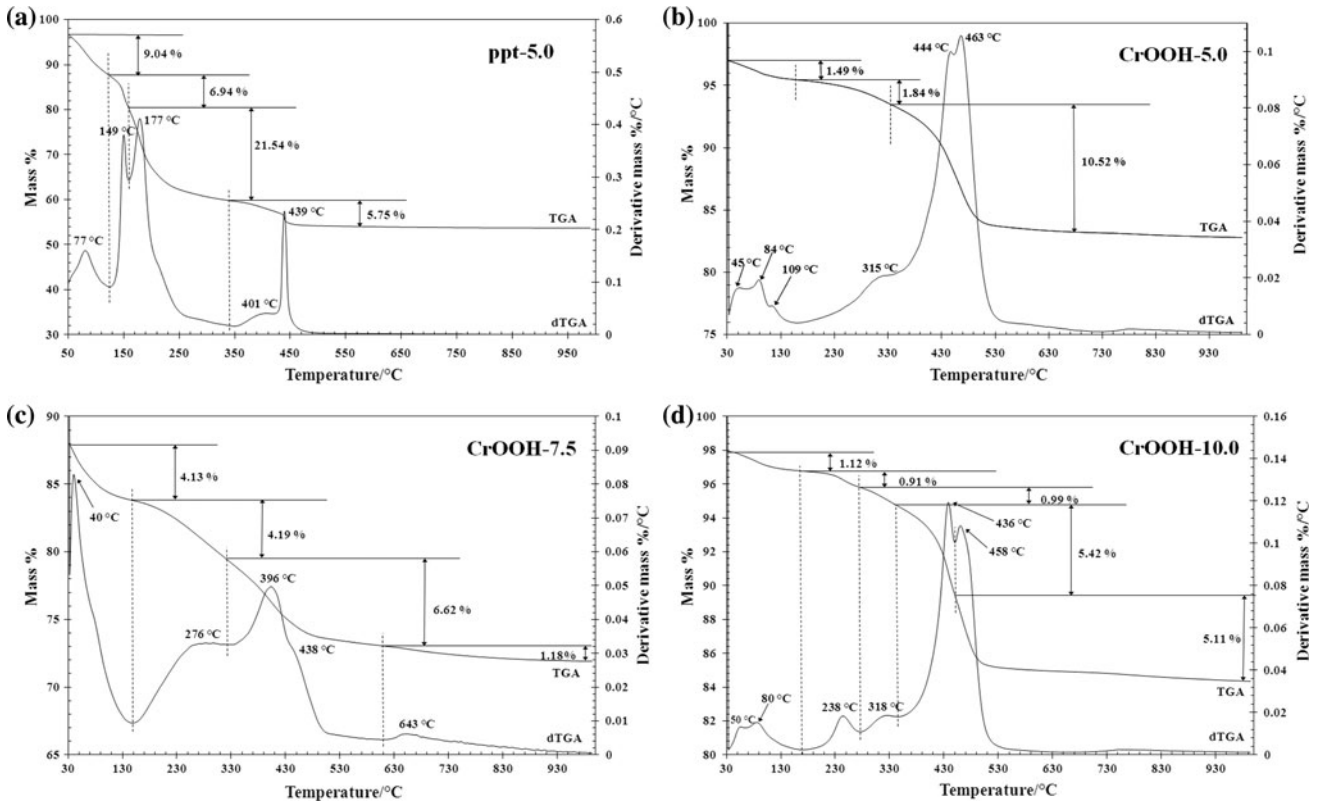

Fig. 8 Thermogravimetric analyses (TGA) of (**a**) ppt-5.0, (**b**) CrO(OH)-5.0, (**c**) CrO(OH)-7.5 and (**d**) CrO(OH)-10.0

Leonard [36] reported that below 200 °C water molecules were eliminated from the amorphous hydroxide precursor precipitated from $Cr(NO_3)_3$ solution with NH_4OH, and a crystalline Cr_2O_3 phase was produced at 400 °C. This finding is in excellent agreement with the results in this study. In the dTG curve of this experiment, the shoulder at 401 °C can be assigned to the dehydration of the small amount of amorphous chromium hydroxide to chromium oxide.

After the HT of the chromium hydroxide gel, the product (noted as sample B) shows a totally different thermal decomposition pattern in Fig. 8b. As confirmed from XRD (Fig. 1), this hydrothermal product is crystalline CrO(OH) nanomaterial. In the thermal study, the major mass loss steps occur at 444 and 463 °C with a total mass loss of 10.52%. These mass loss steps are attributed to the dehydroxylation of the compound according to the reaction $2CrO(OH) \rightarrow Cr_2O_3 + H_2O$. The theoretical mass loss for this reaction is 10.59%, which is consistent with our experimental mass loss of 10.52%. The minor mass losses observed below 110 °C are attributed to water desorption.

Figure 8c presents the thermal analysis of CrO(OH) obtained after 4-days of HT from precipitate at pH = 7.5,

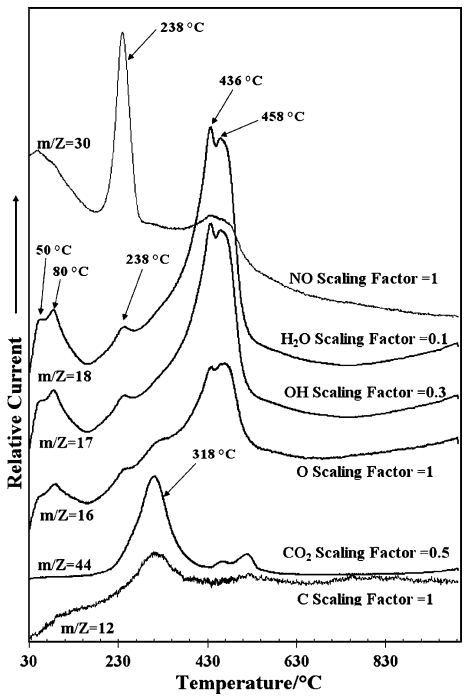

Fig. 9 Mass spectrometric analysis associated with the thermal decomposition process for sample CrO(OH)-10.0

Table 4 Summary of peaks shown in dTG curves for synthesised chromium materials

ppt-5.0 (°C)	CrO(OH)-5.0 (°C)	CrO(OH)-7.5 (°C)	CrO(OH)-10.0 (°C)
77	45, 84, 109	40	50, 80
149, 177			
		276	238
	315		318
401		396	
439	444, 463	438	436, 458
		643	

which is noted as sample C. The dTG curve shows a large band at 396 °C with two broad shoulders.

The main mass loss of sample C at 396 °C is attributed to the dehydroxylation of amorphous chromium hydroxide to crystalline chromium oxide, as discussed above. The shoulder at 276 °C is attributed to the formation of CrO(OH) from chromium hydroxide which was X-ray amorphous. It is suggested that surface formation of CrO(OH) during the heating of chromium hydroxide at lower temperatures occur [30]. Another shoulder peak in the dTG curve of sample C appears at 438 °C. This mass loss is assigned to the dehydroxylation of a small amount of chromium oxy-hydroxide to crystalline chromium oxide.

Sample D synthesised at pH 10.0 shows a similar dTG pattern as sample B. XRD showed these samples had a more crystalline CrO(OH) phase. The dTG curve of sample D shown in Fig. 8d, and the associated mass spectrometric analysis is reported in Fig. 9. The main mass losses at 436 and 458 °C are attributed to the dehydroxylation of CrO(OH) to Cr_2O_3, which is confirmed by the maxima for ion current curves for H_2O, OH and O (Fig. 9). A small mass loss of 0.91% at 238 °C is observed, which is attributed to the decomposition of nitrate impurity. Such decomposition is confirmed by the ion current curves of NO where a maximum at 238 °C is observed. The mass loss step at 318 °C is assigned to the release of CO_2, confirmed by the ion current curves of CO_2 and C.

Peaks shown in dTG curves of the four samples are summarised in Table 4. All the four samples showed a sharp dTG peak around 440 °C, which was due to the dehydroxylation of CrO(OH). Samples B and D, are more crystalline (XRD), show an additional dehydroxylation peak at around 460 °C associated with CrO(OH). Samples A and C show peaks at around 400 °C, which are assigned to the dehydroxylation of amorphous chromium hydroxide. These samples were obtained by precipitation at room temperature from chromium nitrate and ammonia. Similar gel materials have been reported by Milligan [37] and Ratnasamy and neonard [36]. Milligan's study found that there was a certain amount of chromium trihydroxide ($Cr(OH)_3$) in the sample. A mass loss at around 315 °C for samples B and D, but not for sample C, is assigned to the release of CO_2 (identified by MS) from an impurity.

The thermal analysis of the samples up to 1000 °C all were found to transform to a well-crystalline Cr_2O_3 phase (XRD), as shown in Fig. 10. All the diffraction peaks of products were well indexed using a rhombohedral system of lattice for Cr_2O_3, with space group of *R*-3*c* (JCPDS card, No. 01-084-1616). It is noticed that all these thermal products have very high crystallinity and purity, even from the colloidal precipitate (sample A). It is reported that when chromium hydroxide materials are heated, the amorphous material can be converted into crystalline Cr_2O_3 of around 400 °C [36, 52]. However, the thermal

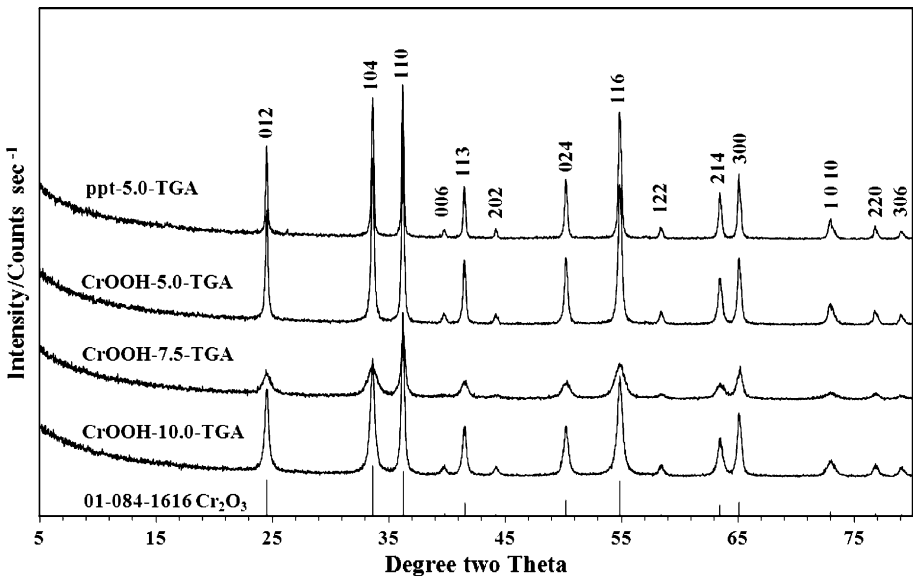

Fig. 10 XRD patterns of products after TGA from ppt-5.0, CrO(OH)-5.0, CrO(OH)-7.5 and CrO(OH)-10.0. XRD patterns from literature: JCPDS card No. 01-084-1616 Cr_2O_3

product from sample C has a slightly lower crystallinity. It is suggested that the pH condition for materials precipitate can affect the crystallinity of the synthesised material.

Conclusions

Chromium oxyhydroxide nanomaterials were obtained by soft-chemistry methods under various conditions. A combination of techniques were used to study morphology and structure of the as-prepared nanomaterials, including XRD, SEM, TEM, BET specific surface area analysis, XPS and thermal analysis. The pH value in precipitate process was proven to be critical for the formation and crystallinity of the synthesised nanomaterials. The CrO(OH) nanomaterials were found to form most easily with an acidic precipitate process. The synthetic chromium oxyhydroxide was identified with a plate-like morphology of $\sim$11 nm in size. N_2 adsorption study is proven as a facile way to provide information on textural properties of the synthesised compounds. XPS measurements for the as-prepared chromium oxyhydroxide nanomaterials allow us to develop a view to determine spectral characteristics and to identify element chemical environment in the compounds. It is also reported that the dehydroxylation of the synthetic chromium oxyhydroxides occurs at $\sim$460 °C, while chromium hydroxide impurities decomposed at $\sim$400 °C.

Acknowledgements The financial and infra-structure support of the Queensland University of Technology Chemistry Discipline is gratefully acknowledged. The Australian Research Council (ARC) is thanked for funding the instrumentation. One of the authors (JY) thanks the Queensland University of Technology for a postgraduate doctoral scholarship. Thanks are also given to Dr. B. Wood for technical and computing support in the XPS study.

References

1. Nofz M, Sojref R, Feigl M, Dressler M, Doerfel I (2009) Keram Z 61(5):272, 274
2. Nofz M, Sojref R, Feigl M, Dressler M, Doerfel I (2009) Keram Z 61(2–3):82
3. Yang X, Peng X, Xu C, Wang F (2009) J Electrochem Soc 156(5):C167
4. Graf W, Brucker F, Koehl M, Troescher T, Wittwer V, Herlitze L (1997) J Non-Cryst Solids 218:380
5. Teixeira V, Sousa E, Costa MF, Nunes C, Rosa L, Carvalho MJ, Collares-Pereira M, Roman E, Gago J (2001) Thin Solid Films 392(2):320
6. Costa MFM, Teixeira V (2007) Int J Photoenergy (1):82327/1
7. Fujikawa J, Hata M, Kokaji K (1998) JP Patent 96-357683 10195646
8. Shigeta K, Goto K (2009) JP Patent 2008-70952 2009230860
9. Rotter H, Landau MV, Herskowitz M (2005) Environ Sci Technol 39(17):6845
10. Carruthers JD, Sing KSW (1967) Chem Ind (45):1919
11. Krivoruchko OP, Zolotovskii BP, Buyanov RA (1977) Tezisy Dokl—Soveshch Kinet Mekh Khim Reakts Tverd Tele, 7th 3:39
12. Rotter H, Landau MV, Carrera M, Goldfarb D, Herskowitz M (2004) Appl Catal B 47(2):111
13. Mosle HG (1969) Metalloberflaeche 23(12):358
14. Clayton CR, Doss K, Warren JB (1983) Passivity of metals and semiconductors: proceedings of the 5th international symposium, p 585
15. Tokunaga K, Sakitani K (1983) Boshoku Gijutsu 32(4):221
16. Chauhan PK, Gaonkar KB, Gadiyar HS (1985) J Electrochem Soc India 34(3):164
17. Yang J, Liu H, Martens WN, Frost RL (2010) J Phys Chem C 114(1):111
18. Yang J, Frost RL (2008) Res Lett Inorg Chem 2008, Article ID 602198. doi:10.1155/2008/602198
19. Yang J, Frost RL, Martens WN (2010) J Therm Anal Calorim 100(1):109
20. Zhao Y, Frost RL, Yang J, Martens WN (2008) J Phys Chem C 112(10):3568
21. Shpachenko AK, Sorokhtina NV, Chukanov NV, Gorshkov AN, Sivtsov AV (2006) Geochem Int 44(7):681
22. Bai Y-L, Xu H-B, Zhang Y, Li Z-H (2006) J Phys Chem Solids 67(12):2589
23. Tang Y, Michel FM, Parise JB, Reeder RJ (2008) Abstracts of papers, 235th ACS national meeting, New Orleans, LA, United States, April 6–10, INOR-056
24. Landau MV, Shter GE, Titelman L, Gelman V, Rotter H, Grader GS, Herskowitz M (2006) Ind Eng Chem Res 45(22):7462
25. Abecassis-Wolfovich M, Rotter H, Landau MV, Korin E, Erenburg AI, Mogilyansky D, Garshtein E (2003) Stud Surf Sci Catal 146:247
26. Abecassis-Wolfovich M, Rotter H, Landau MV, Korin E, Erenburg AI, Mogilyansky D, Gartstein E (2003) J Non-Cryst Solids 318(1,2):95
27. Yang J, Zhao Y, Frost RL (2009) Appl Surf Sci 255(18):7925
28. Cheng H, Liu Q, Yang J, Zhang Q, Frost RL (2010) Thermochim Acta 503–504:16
29. Zhao Y, Yang J, Frost RL (2008) J Raman Spectrosc 39(10):1327
30. Klissurski DG, Bluskov VN (1983) Can J Chem 61(3):457. doi:10.1139/v83-081
31. Giovanoli R, Stadelmann W (1973) Thermochim Acta 7(1):41
32. Simonova LA, Smyshlyaev SI, Tsymbal EP (1973) Izv Vyssh Uchebn Zaved Khim Khim Tekhnol 16(3):334
33. Osmolovskii MG, Andrushchenko LN, Zalitsyna NG (1975) Properties of a series of chromium oxide compounds obtained by a hydrothermal method. Leningr. Gos. Univ, Leningrad, USSR
34. Christensen AN (1976) Acta Chem Scand A A30(2):133
35. Fenerty J, Sing KSW (1976) Proceedings of 1st European symposium on thermal analysis, p 304
36. Ratnasamy P, Leonard AJ (1972) J Phys Chem 76(13):1838
37. Milligan WO (1951) J Phys Colloid Chem 55:497
38. Christensen AN, Hansen P, Lehmann MS (1977) J Solid State Chem 21(4):325
39. Rouquerol F, Rouquerol J, Sing K (1999) Adsorption by powders and porous solids: principles, methodology, and applications. Academic Press, San Diego
40. Gregg SJ, Sing KSW (1982) Adsorption, surface area and porosity, 2nd edn. Academic Press, New York
41. Allen GC, Tucker PM (1976) Inorg Chim Acta 16:41
42. Pollini I (2005) Philos Mag 85(23):2641
43. Wang XY, Wu YS, Zhang L, Yu ZY (2001) Corrosion 57(6):540
44. Liu T, Lu Y (2003) Biaomian Jishu 32(5):20
45. Ikemoto I, Ishii K, Kinoshita S, Kuroda H, Alario-Franco MA, Thomas JM (1976) J Solid State Chem 17(4):425
46. Yuan P, Liu D, Fan M, Yang D, Zhu R, Ge F, Zhu J, He H (2010) J Hazard Mater 173(1–3):614

47. Kendelewicz T, Liu P, Doyle CS, Brown GE (2000) Surf Sci 469(2–3):144
48. Bai Y-l, Xu H-b, Zhang Y, Li Z-h (2007) Guangpuxue Yu Guangpu Fenxi 27(4):675
49. Moffat TP, Latanision RM (1992) J Electrochem Soc 139(7):1869
50. Maurice V, Yang WP, Marcus P (1994) J Electrochem Soc 141(11):3016
51. Sun H, Wu X, Han E-H (2009) Corros Sci 51(11):2565
52. Music S, Maljkovic M, Popovic S, Trojko R (1999) Croat Chem Acta 72(4):789